ELSEVIER

Nuclear Instruments and Methods in Physics Research B 192 (2002) 365–369

NIM B
Beam Interactions with Materials & Atoms

www.elsevier.com/locate/nimb

Measurement and calculation of escape peak intensities in synchrotron radiation X-ray fluorescence analysis

S.X. Kang [a], X. Sun [a], X. Ju [b,*], Y.Y. Huang [b], K. Yao [a], Z.Q. Wu [a], D.C. Xian [b]

[a] *Department of Astronomy and Applied Physics, University of Science and Technology of China, Hefei, Anhui 230036, China*
[b] *Institute of High Energy Physics, Chinese Academy of Sciences, Beijing 100039, China*

Received 5 October 2001

Abstract

In synchrotron radiation X-ray fluorescence experiments, the escape peaks, generating from the Si(Li) solid detector, can disrupt seriously the quantitative and qualitative analysis. In this paper, 14 specimens, such as metals, compounds and plants, have been chosen as objectives to determine the intensities and positions of escape peaks. In all, the characteristic X-ray fluorescence peaks and their escape peaks of 12 elements have been measured. Comparing the experimental values with the standard values, the escape peaks can be discriminated. To calculate the ratios of intensities of the escape peaks and their corresponding characteristic X-ray fluorescence peaks, a simplified Si Kα emergent spherical distribution has been put forward. It is found that the experimental results are in accordance with that of calculation, i.e. both the experimental and theoretical ratios decrease from 1% to 0.1% with the increasing atomic number from 18 to 33 (from 1 to 9 keV in X-ray range).

Keywords: Synchrotron radiation X-ray fluorescence analysis; Si(Li) detector; Escape peak

1. Introduction

Synchrotron radiation X-ray fluorescence (SR-XRF) analysis is being extensively applied in many fields, such as materials science, life science, medical science and environmental science [1–8]. In the conventional XRF measurement, the escape peak would be encountered when a Si(Li) solid detector is commonly used, immediately influencing the identification of trace elements and the calculation of peak area. The escape peak is generated from the Si(Li) solid detector, which is used for measuring the energy of the incident X-ray photons. In brief, when the incident photons entered the Si(Li) detecting device, more than 90% of them are absorbed by Si K shell electrons, and Si Kα fluorescence is yielded in the relaxation process. Once the Si Kα photons escape from the Si(Li) device, the deposit energy in Si(Li) device is decreased by 1740 eV (the photon energy of the Si Kα line) from the initial photon energy. Finally, the escape peak occurs.

As well known, the background (bremsstrahlung spectrum) of the fluorescence spectra excited by X-rays is much lower than that by electron beam. The escape peaks in the fluorescence spectra excited by X-rays can be measured and identified

* Corresponding author. Tel.: +86-10-68235998; fax: +86-10-68186229.
E-mail addresses: jux@ihep.ac.cn, ju.xin@nims.go.jp (X. Ju).

0168-583X/02/$ - see front matter
PII: S0168-583X(02)00491-3

more easily than in that excited by electron beam. In the XRF analysis, these escape peaks may obstruct the quantitative and qualitative analysis. In fact, this phenomenon has been realized in early years [9], but the removal of the escape peak did not included in the conventional XRF analysis programs, such as in AXIL [10,11]. In this paper, we measure the ratios of intensities of the escape peaks and their corresponding characteristic X-ray fluorescence peaks from experiments and compare with the calculated values.

2. Experiments

The XRF experiments were performed at the 4W1A beamline of Beijing Synchrotron Radiation Facility (BSRF), whose energy range of X-rays was 3.5–22.9 keV. The electron beam energy was 2.2 GeV and the beam current was 60–100 mA. The sensitive area on sample of the incident X-rays was adjusted by the slits at the window of the front end of the beamline, which was fixed at 60×60 or 20×20 μm^2 in our experiments. The distance between slit and sample was 100 cm. A Si(Li) solid detector perpendicular to the direction of the incident X-rays was used to measure the fluorescence signals with a distance of 3–10 cm from the samples. The energy resolution of the detector was 165 eV at the Mn Kα line. A 2048 channel MCA was used to record the XRF spectra. In our experiments, the white light was used as the exciting beam. An optical microscope was used to adjust the sample position. 14 specimens were chosen as the objectives. They are: polishing Co, Fe, Ni, Cu and stainless steel sheet; GaAs single crystal; $KMnO_4$, TiO_2, and ZnO powders (analytical purity); $CoCl_2$ film on silicon substrate with a thickness of 1 μm; and four K- and Ca-rich plants (*Sargassum pallidum*, *Tulipa edulis*, *Ceratophyllum demersum* and Antarctic moss).

3. Results and discussion

3.1. Discrimination of escape peak

In the XRF spectra, the positions of the escape peaks can be obtained from the experimental X-ray fluorescence peaks (Fig. 1) and compared with the standard values as shown in Table 1, where $E_{K\alpha}$ is the energy of the main peak and E_{esc} is that of the escape peak from the main peak. It can be seen that the deviation of the experimental

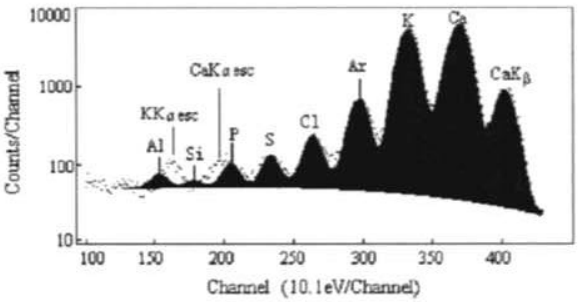

Fig. 1. The AXIL fitting result of *Sargassum pallidum* XRF spectrum.

Table 1
The energy parameters of some elements in the XRF spectra

Element	$E_{K\alpha}$ (eV)	E_{esc} (Standard) (eV)	E_{esc} (Exp.) (eV)
Ar	2958	1218	–
K	3314	1574	1572[a]
Ca	3692	1952	1948[b]
Sc	4091	2351	–
Ti	4511	2771	2748[c]
V	4952	3212	–
Cr	5415	3675	3669[d]
Mn	5899	4159	4247[e]
Fe	6403	4663	4664[f]
Co	6930	5190	5197[g]
Ni	7478	5738	5736[h]
Cu	8048	6308	6308[i]
Zn	8639	6899	6900[j]
Ga	9252	7512	7508[k]
Ge	9886	8146	–
As	10544	8804	8867[k]
Se	11222	9482	–
Sr	11924	10184	–

[a] Experimental average value of *Sargassum pallidum*, *Tulipa edulis*, *Ceratophyllum demersum* and $KMnO_4$.
[b] Experimental average value of *Sargassum pallidum*, *Tulipa edulis*, *Ceratophyllum demersum* and Antarctic moss.
[c] TiO_2.
[d] Stainless steel.
[e] $KMnO_4$.
[f] Fe.
[g] Co and $CoCl_2$.
[h] Ni.
[i] Cu.
[j] ZnO.
[k] GaAs.

[c] TiO_2.

escape peaks from the standard values is less than 1%.

So in the XRF analysis, the discrimination of escape peaks can be carried out in conformity with the peak position (e.g. K $K\alpha_{esc}$ and Ca $K\alpha_{esc}$ of the dotted experimental XRF spectrum). In Fig. 1, the fitted spectrum from the assumed Al, Si, P, S, Cl, Ar, K, Ca elements is also shown as the dark peaks. It can be seen that the deviation of Al, Si, and P peaks is quite large, for example, the peak position of the presumed Al peak is 85 eV lower than the real position of the K $K\alpha_{esc}$ peak (dashed line) in the spectrum, and the P peak 78 eV higher than the Ca $K\alpha_{esc}$, so that these peaks must be canceled. The AXIL fitting of the plant spectrum indicates that it is in good conformity for most strong peaks, induced by Ca, K, Ar, Cl, S elements. Meanwhile, It is found that the intensities of these two escape peaks increase with that of the K, Ca $K\alpha$ lines in the plant samples.

3.2. The measurement of the intensities of escape peaks and their main XRF peaks

The ratios of intensities between escape peaks and their corresponding main characteristic XRF peak can be obtained in the XRF experiments. In our experiments, the AXIL program was used to calculate the area of peaks.

To raise the precision, only the interested region was fitted, in which both the main and escape peaks of the same elements should be included. For the plant samples, the intensity of escape peak was weak, so the average value of several samples has been picked in order to minimize the measurement errors. In our analysis, the counts per channel at both sides of the escape peak were used to determine the linear background that was removed from escape peak.

In Table 2, the experimental values of the intensity ratios between the escape peak and the main XRF peak are listed. Meanwhile, the calculated values of intensity ratios using the Model B mentioned in the next part are also presented. The experimental samples are the same as that in Table 1.

3.3. Calculation of the intensity ratios between the escape peak and the main XRF peak

Suppose that the incident XRF peak intensity of A $K\alpha = 1$, as shown in Fig. 2, the X-ray fluorescence intensity $I(z)^A$ at the depth z of the Si(Li) device is

Table 2
The experimental values of the intensity ratios between the escape peak and the main XRF peak

Element	Intensity of XRF peak (I^A)	Intensity of escape peak (I_e^{Si})	I_e^{Si}/I^A (%) (Exp. value)	I_e^{Si}/I^A (%) (Cal. value)
Ar	–	–	–	1.065
K	231929	2125	0.92 ± 0.06	0.927
Ca	474944	3910	0.82 ± 0.02	0.814
Sc	–	–	–	0.698
Ti	828546	4678	0.56 ± 0.07	0.592
V	–	–	–	0.498
Cr	145898	563	0.38 ± 0.05	0.415
Mn	1970836	6677	0.30 ± 40.0	0.345
Fe	541253	1344	0.25 ± 0.03	0.286
Co	726708	1822	0.25 ± 0.04	0.236
Ni	794323	1464	0.18 ± 0.04	0.196
Cu	265517	438	0.16 ± 0.02	0.162
Zn	640603	788	0.12 ± 0.02	0.134
Ga	485661	496	0.10 ± 00.0	0.112
Ge	–	–	–	0.093
As	229401	216	0.09 ± 0.02	0.078
Se	–	–	–	0.066
Br	–	–	–	0.055

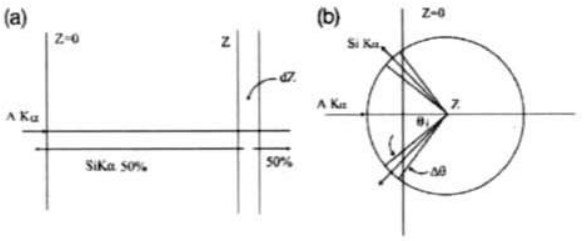

Fig. 2. The schematic of the calculated model: (a) Model A; (b) Model B.

$$I(z)^{\mathrm{A}} = \exp(-\mu_{\mathrm{Si}}^{\mathrm{A}}\rho_{\mathrm{Si}}z)$$

where $\mu_{\mathrm{Si}}^{\mathrm{A}}$ is the mass absorption coefficient of characteristic X-ray fluorescence of an element in silicon. In Table 3, the mass absorption coefficients of some Kα lines in silicon are listed [12]. Here the mass density of silicon $\rho_{\mathrm{Si}} = 2.42$ g/cm^2.

So, the intensity absorbed by a layer dz at the depth z is

$$-\mathrm{d}I(z)^{\mathrm{A}} = I(z)^{\mathrm{A}}\mu_{\mathrm{Si}}^{\mathrm{A}}\rho_{\mathrm{Si}}\mathrm{d}z.$$

$(\gamma_{\mathrm{k}} - 1)/\gamma_{\mathrm{k}}$ is the fraction of the incident photons absorbed by the K-electron of Si, where $\gamma_{\mathrm{k}} = 12.4$ is the jump ratio of the mass absorption coefficient at Si K-edge, and ~92% of the total incident photons was absorbed by K-electron of Si. In the following relaxation, the number of the Si Kα line at the depth z is

$$\mathrm{d}I(z)^{\mathrm{Si}} = -\mathrm{d}I(z)^{\mathrm{A}}[(\gamma_{\mathrm{k}} - 1)/\gamma_{\mathrm{k}}]\omega_{\mathrm{k}},$$

where $\omega_{\mathrm{k}} = 0.043$ is the yield of the Si K line.

Based on the above equation, the angular distribution of emitted the Si Kα line has to be assumed to give the escape ratio as follows:

Model A: Suppose that 50% of Si Kα photons going along the incident direction is absorbed in the Si(Li) device to form the electron–hole pair and counted in the area of main peak; the other 50% going inversely is escaping partly to form the escape peak. Simply, as shown in Fig. 2(a), these escaped Si Kα photons at the depth z emitted perpendicular to the surface of the Si(Li) device, noted as $\mathrm{d}I_{\mathrm{e}}(z)^{\mathrm{Si}}$ is

$$\mathrm{d}I_{\mathrm{e}}(z)^{\mathrm{Si}} = -\mathrm{d}I(z)^{\mathrm{A}}[(\gamma_{\mathrm{k}} - 1)/\gamma_{\mathrm{k}}]\omega_{\mathrm{k}}\exp(-\mu_{\mathrm{Si}}^{\mathrm{Si}}\rho_{\mathrm{Si}}z)/2,$$

where $\mu_{\mathrm{Si}}^{\mathrm{Si}} = 347.2$ cm^2/g is the mass absorption coefficient of characteristic X-ray fluorescence of Si Kα in Si and the factor 1/2 is due to the 50% Si Kα photons going out, so

$$\begin{aligned}\mathrm{d}I_{\mathrm{e}}(z)^{\mathrm{Si}} &= \frac{1}{2}\exp(-\mu_{\mathrm{Si}}^{\mathrm{A}}\rho_{\mathrm{Si}}z)\mu_{\mathrm{Si}}^{\mathrm{A}}\rho_{\mathrm{Si}} \\ &\quad\times[(\gamma_{\mathrm{k}} - 1)/\gamma_{\mathrm{k}}]\omega_{\mathrm{k}}\exp(-\mu_{\mathrm{Si}}^{\mathrm{Si}}\rho_{\mathrm{Si}}z)\mathrm{d}z \\ &= \frac{1}{2}\exp[-(\mu_{\mathrm{Si}}^{\mathrm{A}} + \mu_{\mathrm{Si}}^{\mathrm{Si}})\rho_{\mathrm{Si}}z]\mu_{\mathrm{Si}}^{\mathrm{A}}\rho_{\mathrm{Si}} \\ &\quad\times[(\gamma_{\mathrm{k}} - 1)/\gamma_{\mathrm{k}}]\omega_{\mathrm{k}}\mathrm{d}z.\end{aligned}$$

For the Kα lines listed in Table 1, the Si(Li) device is thick enough to consider the range of the integral of z from 0 to ∞, so

$$\frac{I^{\mathrm{Si}}}{I^{\mathrm{A}}} = \frac{\mu_{\mathrm{Si}}^{\mathrm{A}}}{\mu_{\mathrm{Si}}^{\mathrm{A}} + \mu_{\mathrm{Si}}^{\mathrm{Si}}}\frac{\gamma_{\mathrm{k}} - 1}{\gamma_{\mathrm{k}}}\frac{\omega_{\mathrm{k}}}{2}.$$

Model B: Suppose that the incident photons is along the central axis of the Si(Li) device, as shown in Fig. 2(b), and the Si Kα line at the depth z was emitted uniformly with a spherical distribution. The solid angle between θ_{i} and $\theta_{\mathrm{i}} + \Delta\theta$ in this cone is

$$\mathrm{d}\Omega = \sin\theta_i\frac{\Delta\theta}{2}.$$

Table 3
The mass absorption coefficients of silicon for some Kα-line ($\mu_{\mathrm{Si}}^{\mathrm{A}}$)

A	$\mu_{\mathrm{Si}}^{\mathrm{A}}$ (cm^2/g)
Ar	1045
K	773.8
Ca	578.9
Sc	437.5
Ti	333.9
V	257.2
Cr	199.8
Mn	156.5
Fe	123.7
Co	98.4
Ni	78.9
Cu	63.7
Zn	51.8
Ga	42.4
Ge	34.9
As	28.9
Se	24.1
Br	20.1

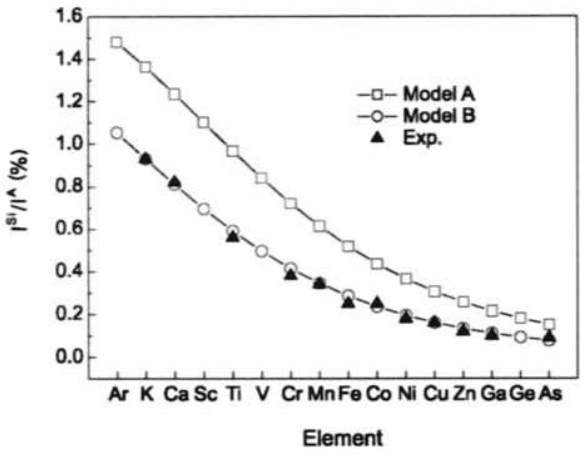

Fig. 3. The relationship between I^{Si}/I^{A} and atomic number Z.

The emitting distance is $z/\cos\theta_i$, the number of escaped photon in $d\Omega$ is

$$dI_e(z)^{Si} = \frac{1}{2}\exp\left[-\frac{\mu_{Si}^{A}+\mu_{Si}^{Si}}{\cos\theta_i}\rho_{Si}z\right]\mu_{Si}^{A}\rho_{Si}\frac{\gamma_k-1}{\gamma_k} \times \sin\theta_i\,\Delta\theta\omega_k\,dz.$$

Given $\Delta\theta = 1°$, the escaped fraction I_e^{Si}/I^{A} can be obtained through summing $\theta_i = 1° - 89°$.

The results of the calculation with both Model A and B are shown in Fig. 3. It is found that the I^{Si}/I^{A} decreases when the atomic number Z increases. With both models, the I^{Si}/I^{A} decrease in one order of magnitude, i.e. for Model A from 1.5% to 0.2%, and for Model B from 1% to 0.1%, respectively. Comparing to the experimental values in Table 2, the calculated values with Model B are in good accordance with a deviation in the range of 1–10%. Obviously, the calculated values with Model A deviated significantly from experimental ones because the angular distribution of the scattering SiKα considered is not suitable.

4. Conclusion

In the analysis of the SR-XRF, the position and intensity of escape peak has to be discriminated in order to identify exactly the composition of elements in various samples. The results of calculation with Model B indicate that the values of the I^{Si}/I^{A} decrease from 1% to 0.1% when the atomic number Z increases from 18 to 33, which is consistent with that of our experiments. For the XRF analysis of the complicated multi-elements system, the calculated values of the I^{Si}/I^{A} can be immediately applied to the correction of the XRF spectrum.

References

[1] J. Osan, S. Torok, A. Rindby, Microscopic X-ray Fluorescence Analysis, in: K.H.A. Janssens, F.C.V. Adams, A. Rindby, Wiley, London, 2000, p. 315.
[2] M.L. Caravlho, C. Casaca, J.P. Marques, T. Pinheiro, A.S. Cunha, X-Ray Spectrom. 30 (2001) 190.
[3] A. Ektessabi, X-Ray Spectrom. 30 (2001) 44.
[4] J.V. Gilfrich, X-Ray Spectrom. 30 (2001) 203.
[5] Y.Y. Huang, L.M. Zhao, Z.G. Wang, H.R. Shao, G.C. Li, Y.R. Wu, W. He, J.X. Lu, R.G. He, Inter. J. PIXE 9 (3–4) (1999) 175.
[6] W.M. Kwiatek, G.L. Long, J.G. Pound, K.R. Peuhl, A.L. Hanson, K.W. Jones, Nucl. Instr. and Meth. B 49 (1990) 561.
[7] X.S. Shen, L.G. Sun, X.B. Yin, L. Zhang, S.X. Kang, Y.Y. Huang, X. Ju, Chinese J. Polar Res. 13 (1) (2001) 50.
[8] C.J. Sparks Jr., Synchrotron Radiation Research, in: H. Winick, S. Doniach, Plenum, New York, 1980, p. 459.
[9] J.L. Campbell, J.A. Maxwell, T. Papp, G. White, X-Ray Spectrom. 26 (1997) 223.
[10] B.X. Yang, Q.T. Lu, J. China Uni. Sci. Technol. 24 (4) (1994) 500.
[11] P. Van Espen, H. Nullens, F. Adams, Nucl. Instr. and Meth. 142 (1977) 243.
[12] R.F.J. Heinrich, Mass absorption coefficients for electron probe microanalysis, in: J.D. Brown (Ed.), 11th International Conference on X-ray Optics and Microanalysis, London, 1986, p. 74.